# An Analytical Approach to the Measurement of Equilibrium Binding Constants: Application to EGF Binding to EGF Receptors in Intact Cells Measured by Flow Cytometry†

Richard A. Stein, John C. Wilkinson, Cheryl A. Guyer, and James V. Staros*

*Department of Biological Sciences, Vanderbilt University, Nashville, Tennessee 37235*

*Received December 12, 2000; Revised Manuscript Received February 27, 2001*

ABSTRACT: In ligand binding studies, ligand depletion often limits the accuracy of the results obtained. This problem is approached by employing the simple observation that as the concentration of receptor in the assay is reduced, ligand depletion is also reduced. Measuring apparent $K_D$'s of a ligand at multiple concentrations of receptor with extrapolation to infinitely low receptor concentration takes ligand depletion into account and, depending on the binding model employed, yields a $K_D$ within the defined limits of accuracy. We apply this analysis to the binding of epidermal growth factor (EGF) to the EGF receptor expressed in intact 32D cells, using a homogeneous fluorescein-labeled preparation of EGF and measuring binding by flow cytometry. Binding isotherms were carried out at varying cell densities with each isotherm fit to the generally applied model with two independent binding sites. Examination of the variation in the $K_D$'s versus cell density yields a high-affinity site that accounts for 18% of the sites and a lower affinity site that accounts for the remainder. However, further examination of these data suggests that while consistent with each individual isotherm, the simple model of two *independent* binding sites that is generally applied to EGF binding to the EGF receptor is inconsistent with the changes in the apparent $K_D$'s seen across varying cell densities.

The epidermal growth factor receptor (*1*) is a member of the ErbB family (*2*), that includes ErbB2/HER2 (*3*), ErbB3 (*4, 5*), and ErbB4 (*6*), and is the prototypical member of the superfamily of transmembrane receptor tyrosine kinases. There are multiple ligands for the ErbB family of receptors (*2*), including EGF (*7*−*9*), TGFα (*10*), betacellulin (*11*), amphiregulin (*12*), epiregulin (*13*), HB-EGF (*14*), and the neuregulins 1−4 (*15*−*20*). ErbB receptor function has been proposed to rely on the formation of multiple combinations of homo- and heterodimers (*21*). In the cell, the extent of dimerization and the composition of dimers most likely depend on the receptors that are expressed, their level of expression, and the ligands that are present. A better understanding of the ligand binding events for the individual receptors and receptor combinations should yield insights on the function of homo- and heterodimeric receptors in signal transduction.

There have been a variety of studies that have examined ligand binding to the ErbB receptors. The most extensively studied is the binding of EGF to the EGF receptor. In most cases, examination of EGF binding to the EGF receptor has suggested that two classes of receptors exist, a high- and a low-affinity class, respectively (*22*−*25*). One hypothesis is that the low-affinity class represents ligand binding to a monomer, whereas the high-affinity class represents preformed dimers (*26*). Within the framework of this hypothesis, one open question is whether the high-affinity class represents a heterodimer or a homodimer of the EGF receptor, since the cell lines that have been used in most binding studies express other members of the ErbB family, specifically ErbB2, which has been shown to be the preferred heterodimerization partner of the other three receptors (*27*). The hypothesis that heterodimerization of the EGF receptor with ErbB2 creates a high-affinity ligand binding site is supported by data indicating that ErbB3 alone binds neuregulin with low affinity, but in the presence of ErbB2 there is both low- and high-affinity binding of ligand (*28, 29*).

The use of a fluorescent ligand and flow cytometry to measure ligand binding was pioneered by Bohn (*30*). This method of measuring ligand binding, further advanced by Sklar et al. (*31*), was first applied to studies of EGF binding to the EGF receptor by Chatelier et al. (*32*). There are several advantages to carrying out a ligand binding assay using flow cytometry. Radioactivity is not required, and it is possible to obtain a homogeneously labeled ligand. There is no need to remove free (unbound) ligand, eliminating the requirement for separation techniques, such as filter binding, gel filtration, or centrifugation, that introduce error and often perturb the binding equilibrium prior to measuring the amount of bound ligand. Lack of a washing or filtering step simplifies the assay; binding is performed in the tubes used in the flow cytometer, thus significantly reducing the time required to perform the assay, even though the equivalent amount of time is required for equilibrium binding conditions. One potential drawback is that the cells need to be in suspension,

† This work was supported in part by grants from the National Institutes of Health (R01 GM55056, R01 DK25489, and T32 GM08320).

* Address correspondence to this author at the Department of Biological Sciences, Vanderbilt University, VU Station B 351634, Nashville, TN 37235-1634. E-mail: james.v.staros@vanderbilt.edu. Phone: (615) 322-4341. Fax: (615) 343-6707.

10.1021/bi002817a CCC: $20.00 
Published on Web 04/26/2001

requiring that adherent cells be detached prior to the assay. Like other fluorescence-based methods, a ligand that is intrinsically fluorescent or has a fluorescent moiety attached to it is required. Once a fluorescent ligand is obtained, the affinity of a panel of nonfluorescent potential ligands can, in principle, be measured by competition binding experiments.[1] While our study is aimed at measuring ligand binding via flow cytometry, the data analysis is applicable to any ligand binding assay, without regard to the method of detection of bound ligand.

To exploit the advantages of using flow cytometry to measure ligand binding to receptors in intact cells, a straightforward analytical approach for the determination of $K_D$'s that takes into account ligand depletion was developed. Further, by exploring the interdependence of cell density, the number of receptors per cell, and the apparent $K_D$'s, a method for testing the adequacy of the generally applied two-independent-site model of EGF binding to the EGF receptor was devised. Our analysis indicates that while individual EGF−EGF receptor binding isotherms can be fit with high statistical accuracy to a model with two *independent* binding sites, this model does not accurately describe the behavior of the EGF−EGF receptor interactions.

## THEORY

The derivations in this section assume either ligand depletion or no ligand depletion, and the subsequent analyses investigate the effect of fitting data affected by ligand depletion with equations that assume no ligand depletion. These analyses form the basis for the subsequent discussion on measuring ligand affinity using flow cytometry. The aim of this section is to describe the binding interaction to either a single receptor population or two independent receptor populations in the absence of any nonspecific binding and without measurement of free ligand in the assay. Discussion of the applicability of competition binding assays for both a one- and two-site model utilizing similar methods is in the Supporting Information.

*One-Site Ligand Binding.* The binding interaction between a ligand and a single receptor site at equilibrium is described by the following:

$$\mathrm{R_F} + \mathrm{L_F} \rightleftharpoons \mathrm{RL}$$

$$K_D = \frac{R_F L_F}{RL}$$

where $K_D$ is the dissociation constant, $R_F$ is the concentration of free receptor, $L_F$ is the concentration of free ligand, and $RL$ is the concentration of ligand bound to the receptor. The equations for conservation of mass are

$$R_T = R_F + RL$$

$$L_T = L_F + RL$$

where $R_T$ and $L_T$ denote the total receptor and ligand concentration, respectively. Substituting the equations for conservation of mass into the equation describing ligand affinity and algebraic manipulation yields

$$RL^2 - (L_T + R_T + K_D)RL + R_T L_T = 0$$

The concentration of ligand bound to receptor, $RL$, is then simply the solution of this quadratic equation with the negative root:

$$RL = \frac{(L_T + R_T + K_D) - \sqrt{(L_T + R_T + K_D)^2 - 4R_T L_T}}{2} \quad (1)$$

Under most conditions, this equation is the most accurate description of equilibrium binding of a ligand to a receptor. Historically, however, eq 1 has rarely been used to analyze equilibrium binding curves. In most studies, $L_F$ has not been replaced in the derivation, yielding the equation:

$$RL = \frac{R_T L_F}{L_F + K_D}$$

This method relies on the accuracy with which the concentration of free ligand is known; however, the concentration of free ligand is not frequently measured; rather it is assumed that $L_F = L_T$, based on the routine assumption that the concentration of receptor-bound ligand, $RL$, is negligible compared to the amount of ligand added, $L_T$. When the assumption $L_F = L_T$ is made, it is assumed that there is no ligand depletion, and

$$RL = \frac{R_T L_T}{L_T + K_{D,app}} \quad (2)$$

where $K_{D,app}$, is not the true dissociation constant, $K_D$, but an apparent dissociation constant. Even under experimental conditions in which the concentration of receptor is less than 10% of the dissociation constant, $R_T \leq K_D/10$, the dissociation constant obtained is still an approximation, but it will be within 10% of the true $K_D$. This equation is useful in that the concentration of ligand−receptor complex is proportional to the total concentration of receptor present, with the proportionality determined by $K_{D,app}$ and the concentration of ligand added, $L_T$; however, binding experiments rarely approach ideal conditions and are often performed without consideration of these inherent assumptions.

*Two-Site Ligand Binding.* Many ligand binding studies have suggested the presence of multiple classes of ligand binding sites. The presence of multiple classes of binding sites is often revealed by the nonlinear plots of data transformed and plotted by the method of Scatchard (bound vs bound/free) (*33*). Several authors have discussed appropriate methods and potential difficulties in obtaining binding parameters from these nonlinear plots (*34*−*37*). There are several modes of ligand binding that could lead to nonlinear Scatchard plots. One of the simpler models consists of two noninteracting receptor classes, described by

$$\mathrm{R_F} + \mathrm{L_F} \rightleftharpoons \mathrm{RL},\ \mathrm{S_F} + \mathrm{L_F} \rightleftharpoons \mathrm{SL}$$

$$K_{DR} = \frac{R_F L_F}{RL},\ K_{DS} = \frac{S_F L_F}{SL}$$

where R and S denote two independent receptor classes:

[1] See Supporting Information.

either two different receptors that both bind the ligand, or the same receptor that binds the ligand with two different and independent affinities. While these are considered independent binding sites in relation to their ligand binding properties, the fraction bound for each class is not independent, but will depend on the amount of each receptor class present and on the amount of ligand added. This can be seen by accounting for mass balance:

$$R_T = R_F + R_L$$

$$S_T = S_F + SL$$

$$L_T = L_F + RL + SL$$

One can solve for RL and SL:

$$RL = \frac{R_T L_F}{L_F + K_{DR}} \text{ and } SL = \frac{S_T L_F}{L_F + K_{DS}} \quad (3)$$

and substitute into the equation for $L_T$ to obtain an equation for $L_F$. This equation is a cubic equation like the one obtained for the one-site competition case (see Supporting Information) and can be solved similarly (*38*) to yield:

$$L_F = -\frac{a}{3} + \frac{2}{3}\cos\left(\frac{\theta}{3}\right)\sqrt{a^2 - 3b} \quad (3a)$$

$$\theta = \arccos\frac{-2a^3 + 9ab - 27c}{2\sqrt{(a^2 - 3b)^3}}$$

$$a = K_{DR} + K_{DS} + R_T + S_T - L_T$$

$$b = K_{DS}(R_T - L_T) + K_{DR}(S_T - L_T) + K_{DR}K_{DS}$$

$$c = -K_{DR}K_{DS}L_T$$

Equation 3a can then be used to solve for *RL* and *SL* to obtain the concentration of receptor-bound ligand. The above derivation makes no assumptions about the extent of ligand depletion. Assuming that there is no ligand depletion, $L_T = L_F$, the total bound reduces to

$$\text{BOUND} = RL + SL = \frac{R_T L_T}{L_T + K_{DR,app}} + \frac{S_T L_T}{L_T + K_{DS,app}} \quad (4)$$

This equation is simply the sum of independent binding sites (cf. eq 2), and the amount bound to each subclass is independent of the presence of the other class of receptor. These two derivations can be used to examine the effect of ligand depletion on the determination of the dissociation constants for ligand binding to two independent classes of receptors.

## METHODS

*Simulations and Fitting.* To ascertain the effects of fitting experimental data assuming that there is no ligand depletion, data were simulated with the equations in which ligand depletion is taken into account and then fit with equations in which it is assumed that there is no ligand depletion. Theoretical data were generated using eqs 1 and 3 in the spreadsheet Quatro Pro (Corel). These data were then imported into Prism (GraphPad Software) and fit using built-in functions corresponding to eqs 2 and 4.

*Materials.* Restriction enzymes and T4 DNA ligase were from New England Biolabs. pCDNA3.1(−) was from Invitrogen. Sequanase Kit 2.0 was from U.S. Biochemical, and Sequitherm EXCEL II sequencing kit was from Epicenter Technologies. G418 sulfate was from Mediatech. Protein A−Sepharose CL-4B, enhanced chemiluminescence (ECL) reagents, and horseradish peroxidase (HRP)-conjugated donkey anti-rabbit IgG were from Amersham Pharmacia Biotech. Fetal bovine serum (FBS) was from Gibco BRL. Ab 528 and Ab 1005, both directed against the EGF receptor, were from Santa Cruz Biotechnology. Glycerol was from Fisher. Sodium dodecyl sulfate (SDS) was from Serva. Nitrocellulose membranes were from Schleicher & Schuell. Fluorescein isothiocyanate (FITC)-conjugated goat anti-mouse $IgG_{2a}$ was from Southern Biotechnology Associates. Paraformaldehyde was from Electron Microscopy Sciences. All other reagents were ACS reagent grade or better.

*Construction of H22Y-mEGF.* A plasmid, pIN-II-ompA3-H22Y-mEGF, encoding H22Y-mEGF was constructed using the approach previously described for Y3K,H22Y-mEGF (*39*), except that only a single synthetic oligonucleotide, 5N-GGTGTTTGCTATGTACATCGAATCT-3N, was employed.

*Expression and Purification of H22Y-mEGF.* Following transformation of *E. coli* HB101 with the pIN-III-ompA3-H22Y-EGF plasmid, the expression and purification of H22Y-mEGF were carried out largely as previously described for Y3K,H22Y-mEGF (*39*). Briefly, bacteria were grown to mid-log phase, induced by addition of isopropyl $\beta$-D-thiogalactopyranoside (IPTG) to 200 $\mu$M, harvested by centrifugation, and osmotically shocked to release periplasmic proteins, including H22Y-mEGF. The osmotic shock fluid was lyophilized and dissolved in water. H22Y-mEGF was purified from other periplasmic proteins by reversed-phase HPLC (RP-HPLC) using a 10 × 100 mm Poros R2/H column with 0.1% triethylamine/acetate (pH 6.0) in 95:5 water/acetonitrile (buffer A) and 0.1% triethylamine/acetate (pH 6.0) in 50:50 water/acetonitrile (buffer B) as mobile phases. The solvent delivery system consisted of a Waters 600E system, and the absorbance was monitored at 280 nm with a Waters 486 tunable absorbance detector. For each HPLC run, the column was equilibrated with 100% buffer A, and proteins were eluted using a 2 min linear gradient of 0−100% buffer B at a flow rate of 12 mL/min. The peak containing H22Y-mEGF was hand-collected and lyophilized. The lyophylized protein was redissolved in water and further purified using a 4.6 × 220 mm Brownlee Aquapore RP-300 C-8 column with 0.1% trifluoroacetic acid (TFA) in water (buffer C) and 0.1% TFA in 20:80 water/acetonitrile (buffer D) as mobile phases. The solvent delivery system consisted of two Waters 510 pumps, and the absorbance was monitored at 220 and 280 nm with a Waters 490E detector, with the system controlled from a Maxima 820 workstation. For each HPLC run, the column was equilibrated with 95:5 buffer C/buffer D, and the products were eluted with a 70 min linear gradient of 5−50% buffer D at a flow rate of 1 mL/min. The H22Y-mEGF peak was hand-collected and lyophilized. The lyophilized protein was dissolved in water and quantified by its absorbance at 280 nm [$\epsilon_{280} = 18\,700\ \text{cm}^{-1}\,\text{M}^{-1}$ (*40*)].

*Preparation and Purification of Fluorescein Isothiocyanate Labeled H22Y-mEGF (F-EGF).* Labeling of H22Y-mEGF with fluorescein isothiocyanate was carried out as previously described for wt-mEGF (*41*). The homogeneity of the HPLC-

purified peak was verified in an analytical run using the same gradient. The stoichiometry of the labeled species was verified to be 1:1 by matrix-assisted laser desorption ionization time-of-flight mas spectroscopy (MALDI-TOF MS). The lyophilized F-EGF was dissolved in 5 mM Tris, pH 7.4, and the concentration was quantified from the absorbance using $\epsilon_{280} = 36\,000\ cm^{-1}\ M^{-1}$. This extinction coefficient was used to correct for the contribution of fluorescein to the absorbance at 280 nm (*41*).

*Construction of EGF Receptor Expression Plasmid.* The pXER construct (gift of G. N. Gill, University of California at San Diego) was digested with *Xba*I and *Hin*dIII to generate a full-length EGFR cDNA fragment. This fragment was ligated into the multiple cloning site of the mammalian expression vector pCDNA3.1(−) using T4 DNA ligase to generate the pCER construct. Correct insertion of EGF receptor cDNA was confirmed by dideoxynucleotide sequencing using the SequiTherm EXCEL II sequencing kit according to the manufacturer's instructions.

*Cell Culture.* The IL-3-dependent cell line 32D (obtained from G. Carpenter, Vanderbilt University) was maintained in RPMI-1640 containing 15% FBS and 5% WEH1-3B conditioned medium (as a source of IL-3). Cells were grown at 37 °C in an atmosphere of 5% $CO_2$/95% air.

*Transfection.* 32D cells ($1 \times 10^7$) were transfected by electroporation using 10 $\mu$g of circular pCER DNA. Electroporation was carried out using a BioRad GenePulser II electroporator set at 950 $\mu$F and 300 V. Cells were allowed to recover in RPMI-1640/15% FBS/5% WEH1-3B conditioned medium for 18 h prior to selection by the addition of 750 $\mu$g/mL G418. Clonal cell lines were established by serial dilution in 24-well microtiter plates to a final titer of <1 cell/well. One clone, designated WT3, was selected for these studies.

*Cell Lysis.* Saturated cultures of 32D cells ($1 \times 10^6$ cells/mL) were harvested by centrifugation at 2500*g* for 4 min and washed twice in $Ca^{2+}$,$Mg^{2+}$-free phosphate-buffered saline (CMF-PBS: 137.0 mM NaCl, 8.0 mM $Na_2HPO_4$, 2.7 mM KCl, 1.5 mM $KH_2PO_4$). Cells ($1 \times 10^7$) were lysed by resuspension in 1.0 mL of TGH lysis buffer [150 mM Hepes, pH 7.5, 1% Triton X-100, 10% glycerol, 1 mM ethylene glycol bis($\beta$-aminoethyl ether)-*N*,*N*,*N*′,*N*′-tetraacetic acid (EGTA), 1 mM $Na_3VO_4$, 0.1 mM phenylmethylsulfonyl fluoride (PMSF), 10 $\mu$g/mL aprotinin, and 10 $\mu$g/mL leupeptin] at 4 °C for 20 min with rocking. Lysates were cleared by centrifugation at 16000*g* for 10 min at 4 °C and stored at −70 °C until use.

*Immunoprecipitation and Immunoblotting.* Protein A−Sepharose CL-4B was incubated overnight at 4 °C with TGH buffer containing the EGF receptor antibody 528, directed toward the extracytoplasmic domain of the receptor (2 $\mu$g of Ab/30 $\mu$L of hydrated beads). The resin was washed 3 times with cold TGH buffer, added to cell lysates (1 mg of total protein/30 $\mu$L of beads), and incubated with rocking overnight at 4 °C. Immunoprecipitates were washed 3 times with TGH, and bound proteins were eluted from the resin by treatment with 1× Laemmli sample buffer (62.5 mM Tris·HCl, pH 6.8, 2% SDS, 10% glycerol, 50 mM dithiothreitol, and 0.001% bromophenol blue) and heating for 5 min at 95 °C. Eluted proteins were separated by SDS/polyacrylamide gel electrophoresis [6% gel, (*42*)] prior to transfer to nitrocellulose membranes. EGF receptor was detected by incubating membranes with the EGF receptor antibody 1005 (1:3000 dilution), followed by secondary incubation with HRP-conjugated donkey anti-rabbit IgG (1:1000 dilution). Proteins were visualized by ECL using Kodak X-Omat AR film.

*Determination of EGF Receptor Expression in Intact Cells.* 32D cells were harvested by centrifugation at 2500*g* for 4 min and washed twice in stain buffer (CMF-PBS containing 5% heat-inactivated FBS). Cells were resuspended at $5 \times 10^6$ cells/mL in stain buffer containing 10 $\mu$g/mL Ab 528 and incubated for 20 min at 4 °C. Following incubation, cells were harvested and washed once with stain buffer prior to resuspension at $5 \times 10^6$ cells/mL in stain buffer containing 12.5 mg/mL FITC-conjugated goat anti-mouse $IgG_{2a}$. After incubation for 20 min at 4 °C in the dark, cells were harvested and washed once with stain buffer prior to resuspension at $1 \times 10^6$ cells/mL in stain buffer containing 1% paraformaldehyde. Flow cytometry was performed using a Becton-Dickson FACScan model flow cytometer with CellQuest software.

*Ligand Binding Experiments.* F-EGF was serially diluted to obtain 2× stocks of the final concentrations used (0.001−10 nM). WT3 cells were harvested by centrifugation and resuspended in CMF-PBS + 0.1% BSA at the appropriate 2× cell densities, such that the final binding assay densities ranged from $2.0 \times 10^5$ to $1.3 \times 10^6$ cells/mL. An equal volume (200 $\mu$L) of cell suspension was added to flow cytometry tubes that contained F-EGF (200 $\mu$L). The densities of cells in the assay tube were measured using a Coulter cell counter (model Z1). The tubes were incubated on ice for 2 h with rocking, and the fluorescence was measured in the flow cytometer as described above. Nonspecific binding was measured using a 50-fold excess of unlabeled EGF and was subtracted from total binding to obtain specific binding. The binding constants and estimated standard deviations for these parameters were obtained by fitting the binding isotherms using the built-in one- and two-site binding models in Prism.

## RESULTS

While the derivations under Theory are basic, they are vital for understanding the issues involved in carrying out any ligand binding experiment. Thus, the issues raised below, though directed toward measuring ligand binding using flow cytometry, are applicable to analyzing binding isotherms obtained by other methods. For a typical flow cytometry experiment, cells are harvested and incubated with the fluorescent ligand until steady-state binding is reached. These incubations can be carried out in the tubes that are appropriate for a particular flow cytometer and optimized for variables such as binding medium, temperature, agitation, and time. The flow cytometer detects fluorescence per event, generally set up to be the passage of a single cell across the optical window of the instrument, with the data output as a histogram of the number of events of a measured fluorescence value (fluorescence per cell) (Figure 1A). This histogram is then averaged to obtain a mean fluorescence that is a measure of the amount of ligand bound per cell. The mean fluorescence values for each added ligand concentration plotted versus the added ligand concentration yields a binding curve (Figure 1B).

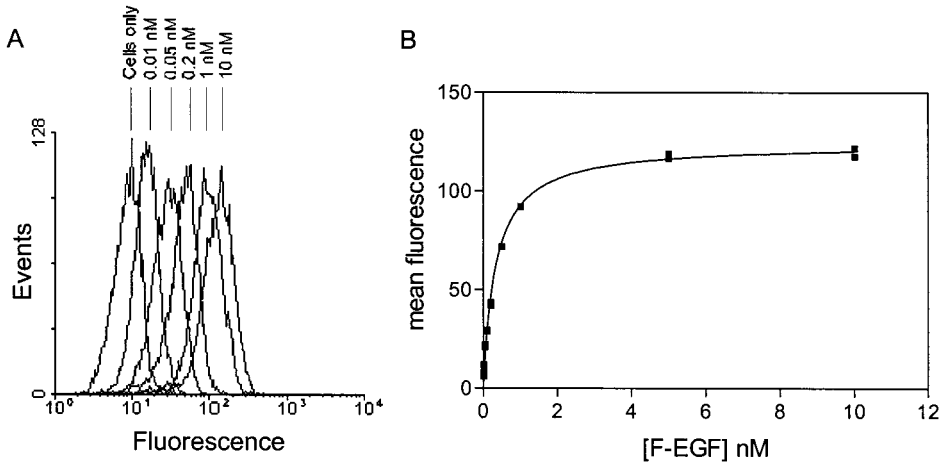


FIGURE 1: Flow cytometry data and ligand binding. (A) Plot of the histograms from flow cytometry for cells at $9.7 \times 10^5$ cells/mL equilibrated with several concentrations of fluorescein-labeled EGF (F-EGF). (B) Binding isotherm of duplicates of F-EGF to EGF receptor expressed in the 32D hematopoietic cell line. The solid line is a fit of the data to eq 2 with $K_{D,app} = 0.34$ nM.

*One-Site Binding.* Previous reports using a fluorescent ligand and flow cytometry noted that the curves obtained using this method were dependent on the cell density used in the experiment (*31*, *32*), implying that the assumption $L_F = L_T$ is not valid and therefore the binding isotherms are more accurately described by eq 1 than by eq 2. To fit the data to eq 1, bound ligand must be expressed as a concentration rather than in arbitrary fluorescence units. Standards have been used to convert arbitrary mean fluorescence units into units of concentration (*43*, *44*); however, the results obtained can depend on the standard used for the calibration (*43*; data not shown) and can vary by 3-fold or more. Moreover, the $K_D$ obtained from the normalized data will depend on the calculated number of receptors per cell, and thus the measured $K_D$ could significantly deviate from the true dissociation constant, depending on any inaccuracy in measuring the number of receptors per cell. We describe here a general method for carrying out ligand binding experiments, utilizing flow cytometry to obtain $K_D$'s, that requires no conversion of fluorescent units to concentrations, no data normalization, and minimal data manipulation.

Typically, binding experiments utilizing cells are carried out by incubating cells with increasing concentrations of ligand. Depending on the number of receptors per cell and the number of cells, use of eq 2 could yield a $K_{D,app}$ that is not a good approximation of the true $K_D$. If the average receptor concentration, i.e., the number of cells per unit volume times the number of receptors per cell, is controlled, that concentration can be set to less than 10% of the expected $K_D$ value. Under these conditions, $L_T = L_F$ is a reasonable assumption, and application of eq 2 would yield a $K_{D,app}$ that would be a good approximation of $K_D$ (data not shown). However, if the number of receptors per cell is not known, then the extent of ligand depletion could be significant, and use of eq 2 under such conditions would lead to a $K_{D,app}$ that could be a poor approximation of the true $K_D$. This raises the question of how to carry out the experiment without knowing a priori the number of receptors per cell.

As noted above, binding isotherms are dependent on cell density. As a consequence of this dependence on cell density, two approaches can be employed to measure $K_D$. One method would be to generate a family of binding isotherms with decreasing cell densities. As the cell density is decreased, there is less ligand depletion, and the $K_{D,app}$ becomes a better approximation of the true $K_D$. As ligand depletion becomes negligible, the changes in $K_{D,app}$ would be on the order of the error in the experiment (10%). At this point, the condition that $R_T \leq K_D/10$ would have been met, and repetition of the experiment using the lowest cell density would yield a reasonably accurate value for $K_{D,app}$.

Similarly, a second method takes into account that the $K_{D,app}$ obtained using eq 2 becomes a better approximation for the true $K_D$ at lower receptor concentrations. In a flow cytometry experiment, it is straightforward to measure binding isotherms for three to four different cell densities, e.g., between $2.5 \times 10^5$ and $1.0 \times 10^6$ cells/mL, and the $K_{D,app}$ for each curve can be determined. The intrinsic $K_D$ value and an estimate of the number of receptors per cell can then be subsequently obtained by plotting the $K_{D,app}$ values versus the cell densities (Figure 2). The *y*-intercept from this plot is equivalent to the intrinsic $K_D$, and the slope is a measure of the number of receptors per cell. In Figure 2, data were simulated for four cell densities using two different $K_D$'s and varying the number of receptors per cell. In the left-hand panels (Figure 2A,C), the number of receptors per cell was varied from 10 000 to 100 000 for two different $K_D$ values, 0.25 nM (Figure 2A) and 1 nM (Figure 2C). For all of these data, the *y*-intercepts are equivalent to the $K_D$'s used to generate the data, and the slopes of the curves increase with the number of receptors per cell. As the number of receptors per cell is further increased (Figure 2B,D), the slope also continues to increase; however, the *y*-intercepts no longer correspond to the $K_D$'s used to generate the data, and the *y*-intercepts become overestimates of binding affinity. This is caused by ligand depletion that occurs under conditions of high receptor numbers and high affinity with the consequence that the data are no longer fit by a straight line. The true $K_D$ can be obtained by fitting the data to a second-order equation ($ax^2 + bx + c$) where the *y*-intercept, *c*, is equivalent to the true $K_D$, though in most experimental cases the noise in the four data points would preclude effective application of a second-order equation.

One question that arises from this analysis is how to determine if there is significant ligand depletion and, as a result, whether the *y*-intercept from a $K_{D,app}$ vs cell density

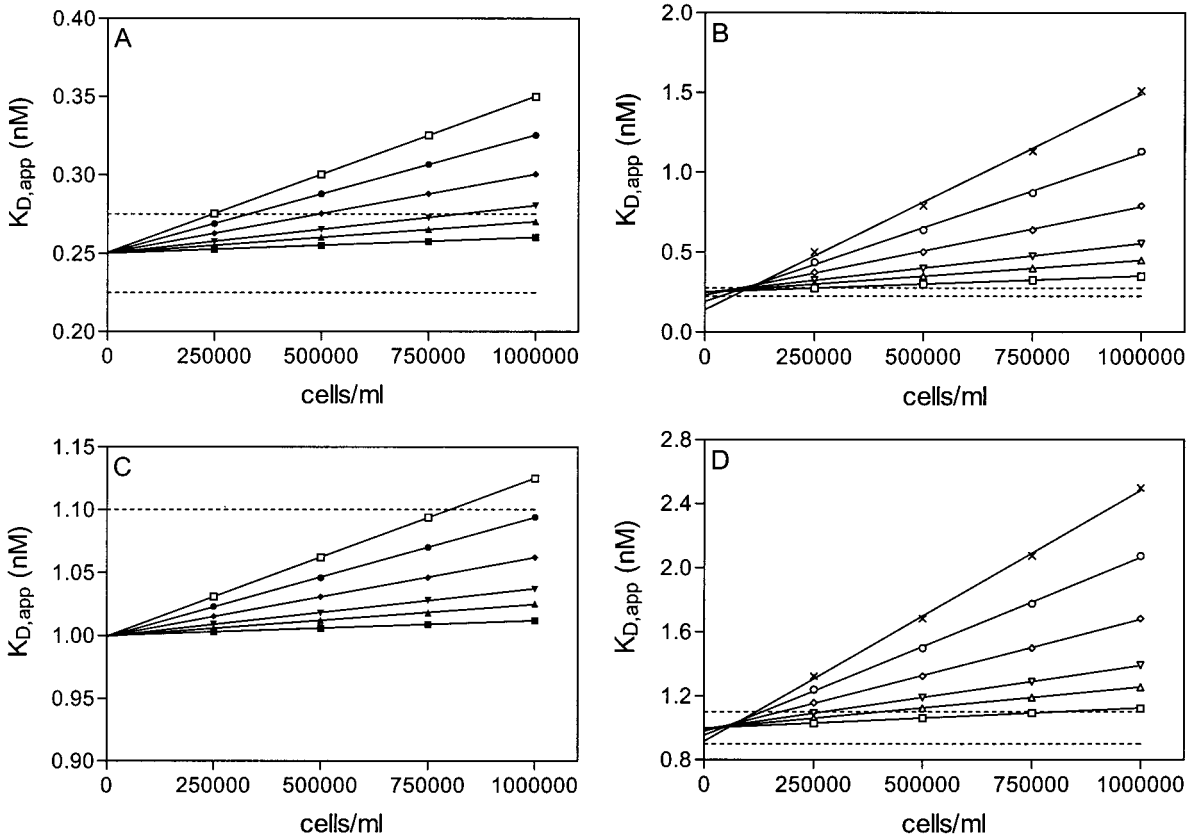


FIGURE 2: Theoretical plots of $K_{D,app}$ versus cell density. Hypothetical data were generated using eq 1 and fit using eq 2. Panels A and B are for $K_D = 0.25$ nM; panels C and D are for $K_D = 1$ nM. The various plots reflect different levels of receptor expression and correspond to 10 000 (■), 20 000 (▲), 30 000 (▼), 50 000 (◆), 75 000 (●), and 100 000 (□) receptors per cell in panels A and C and 100 000 (□), 200 000 (△), 300 000 (▽), 500 000 (◇), 750 000 (○), and 1 000 000 (×) receptors per cell in panels B and D. The dashed lines correspond to ±10% of the value of the $K_D$. The *y*-intercept is equivalent to the $K_D$, and the slope is proportional to the number of receptors per cell.

plot yields an erroneous measure of the $K_D$ for ligand binding. To answer this question, the $K_{D,app}$ obtained at 250 000 cells/mL ($K_1$) is compared to the $K_{D,app}$ obtained at 1 000 000 cells/mL ($K_2$). If $K_2$ is twice or more as large as $K_1$ (e.g., Figure 2B, 1 000 000 receptors per cell), the *y*-intercept from the linear fit is no longer an accurate measure of the true $K_D$ and will deviate from the true $K_D$ by greater than 10% (falling outside the dashed line). A $K_D$ of 0.25 nM can be determined within 10% error for a single class of receptors when receptor expression levels are as high as 500 000 receptors per cell, a value well within most physiological cases. As the $K_D$ increases, the number of receptors per cell that can be tolerated, while ensuring that the *y*-intercept will remain within 10% error, will also increase; e.g., when the $K_D$ is 1 nM, the number of receptors per cell can be as high as 1 000 000. Conversely, as the $K_D$ decreases (higher affinity), then the number of receptors per cell that can be tolerated will decrease. In cases where high receptor expression leads to $K_2 \geq 2 \times K_1$, reducing the cell concentrations while maintaining the same ligand concentrations should restore the linear relationship between $K_{D,app}$ and cell concentration, yielding a *y*-intercept within 10% error of the true $K_D$. Examination of Figure 2 also indicates that when $K_2 \approx K_1$ as a consequence of low affinity and/or very few receptors per cell, a condition reflected by little slope in the $K_{D,app}$ versus cell density plot, there is very little ligand depletion and all values of $K_{D,app}$ should be within 10% of the true $K_D$.

While it is apparent that the slope of the $K_{D,app}$ versus cell concentration plot is sensitive to the number of receptors per cell, there is no straightforward way to parametrize the slope in terms of receptor number. Numerous simulations varying the $K_D$ and the number of receptors per cell were carried out, and the slopes from the linear regressions of plots of $K_{D,app}$ versus cell density plots were calculated. These slopes were then plotted against the $K_D$ values used in generating the data (Figure 3). The family of curves obtained for the slope as a function of $K_D$ at different numbers of receptors per cell can then be used to estimate the number of receptors per cell in ligand binding experiments involving a single class of receptors. As discussed above, analysis of the binding isotherms at the various cell densities yields $K_{D,app}$'s that are then plotted versus cell density. After fitting these data to a straight line, the slope and intercept are used in conjunction with Figure 3 to estimate the number of receptors per cell. First, a horizontal line is drawn from the *y*-axis, corresponding to the value of the slope, and a vertical line is drawn from the *x*-axis, corresponding to the value of the intercept, $K_D$. By comparing the intersection of these two lines relative to the lines based on different values of receptors per cell, the number of receptors per cell in the experiment can be approximated.

A second method of determining the number of receptors per cell is to use eq 1 to simulate four binding isotherms (250 000−1 000 000 cells/ mL) using the $K_D$ determined from the $K_{D,app}$ versus cell density plot and a chosen number

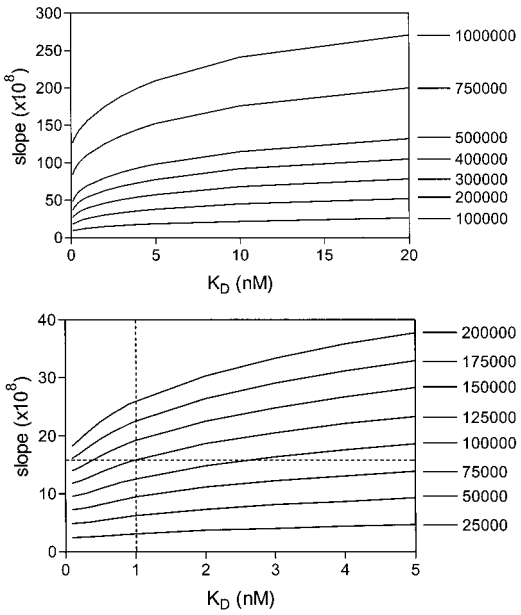


FIGURE 3: Plots to determine the number of receptors per cell. Shown are curves of the slope from linear regressions of $K_{D,app}$ versus cell density for various $K_D$'s at various receptor expression levels. To determine the number of receptors per cell from a binding experiment, lines are drawn corresponding to the slope and the $K_D$ obtained from the $K_{D,app}$ versus cell density plot. The point of intersection of these two lines is a measure of the number of receptors per cell. In the figure is an example showing that a $K_D$ of 1 nM and a slope of $16 \times 10^{-8}$ nM/(cells/mL) would correspond to ~125 000 receptors per cell (dashed lines).

of receptors per cell. The $K_{D,app}$ values from these four isotherms are obtained using eq 2. These $K_{D,app}$ values are then plotted versus cell density and compared to the experimental data. This method is then repeated with iterative changes of the number of receptors per cell until there is convergence of the simulated data with the experimental data.

These two methods do not obtain the receptor number directly from the asymptote of the binding isotherm as in an assay using a radio-labeled ligand. Generation of the data used to obtain the slopes plotted in Figure 3 was carried out at a wide range of effective receptor concentrations relative to binding affinity. Subsequent tests on the use of this figure to obtain the number of receptors per cell yielded accurate estimates (within 10%) of the number of receptors per cell. Use of the second method yielded slightly better estimates, though the small increase in the accuracy was not necessarily offset by the additional time that is required. The accuracy of these methods is achieved by explicitly taking into account the effects of ligand depletion. As a result, the estimate of the number of receptors per cell is accurate regardless of ligand affinity or the effective receptor concentration.

*Two-Site Binding.* The approach of measuring binding at multiple cell densities can be extended to the case of two independent receptor classes. We simulated data with several different high- and low-affinity classes, varying the ratios of the two receptor classes while maintaining the same total number of binding sites. Simulated data were generated with eq 3 using varying cell densities and were fit with eq 2 to examine the effect that fitting two-site data with a one-site model has on the apparent $K_D$ (Figure 4A). It is apparent that increasing the affinity of the high-affinity site (from $K_{D1} = 0.05$ to $K_{D1} = 0.025$), while maintaining the number of total binding sites and proportion of each site, results in an increase in the apparent affinity of the ligand for the receptor, evidenced by comparison of the *y*-intercepts from the left and right panels of Figure 4A. The $K_{D,app}$'s appear to be fairly linear with cell concentration, similar to the one-site case. However, the intercept of any one plot does not correspond to any identifiable combination of the two affinities used to generate the data, and use of the slope with Figure 3 will greatly overestimate the number of receptors per cell.

The simulated data were also fit with eq 4 to obtain the two $K_{D,app}$'s and the fractions of the two receptor populations ($R_T$ and $S_T$) (Figure 4B). This method yielded fractional receptor populations within 10% error and, for the low-affinity site, a $K_D$ within 10% of the value used to generate the data. On the other hand, only one of the fits yielded a *y*-intercept for the high-affinity $K_D$ that was within 10% of the value used to generate the data, though all six fits fell within 25% error. The larger degree of error for the high-affinity site results from significant ligand depletion. While the use of multiple cell densities yields high-affinity $K_D$'s that are less accurate than desired, this method is generally more accurate than using a single cell density where the obtained $K_D$ can deviate from the intrinsic value by severalfold (Figure 4). More accurate determination of the high-affinity $K_D$ could, in principle, be achieved by analysis of the data with eq 3, which explicitly takes into account ligand depletion, but this requires knowledge of the conversion of mean fluorescence to concentration of ligand bound to receptor. Even in cases in which the correspondence between concentration and fluorescence of the ligand *in solution* is known, the correspondence between mean fluorescence and the concentration of *bound* ligand is, in general, difficult to determine accurately, and any errors in this determination will lead to errors in the $K_D$ determination.

*EGF Receptor Expression.* The 32D cell line does not express any of the four members of the ErbB receptor family (*45*). Previous use of this cell line to express ErbB receptors has utilized a retroviral promoter (*45*−*48*). In the current study, the EGF receptor was expressed using pCDNA3.1, which had been previously used in this cell line to express an EGF receptor/JAK kinase chimera (*49*). After selection, clones were established by dilution to obtain single cells. Clonality was assayed by flow cytometry (data not shown), and monoclonal lines were selected for further study. Expression of the EGF receptor was also verified by immunoblot analysis (data not shown). One monoclonal line, designated WT3, was then used for the subsequent analysis of ligand binding to the EGF receptor.

*F-EGF Binding.* The simulations described above were used in devising an experimental protocol for measuring the affinity of F-EGF for the EGF receptor. Twenty point binding isotherms were carried out on varying cell densities of WT3. Specifically bound F-EGF was obtained by subtracting nonspecific F-EGF, which includes F-EGF nonspecifically interacting with the cell and free F-EGF that is in the annulus around the cell that is considered bound to the cell by the flow cytometer, from total F-EGF bound. This nonspecific binding varied from less than 1% of the total bound at the lowest F-EGF concentration to less than 10% at the highest F-EGF concentration. There was little difference in binding constants obtained using the corrected or uncorrected data, indicative of the small nonspecific binding that occurs in

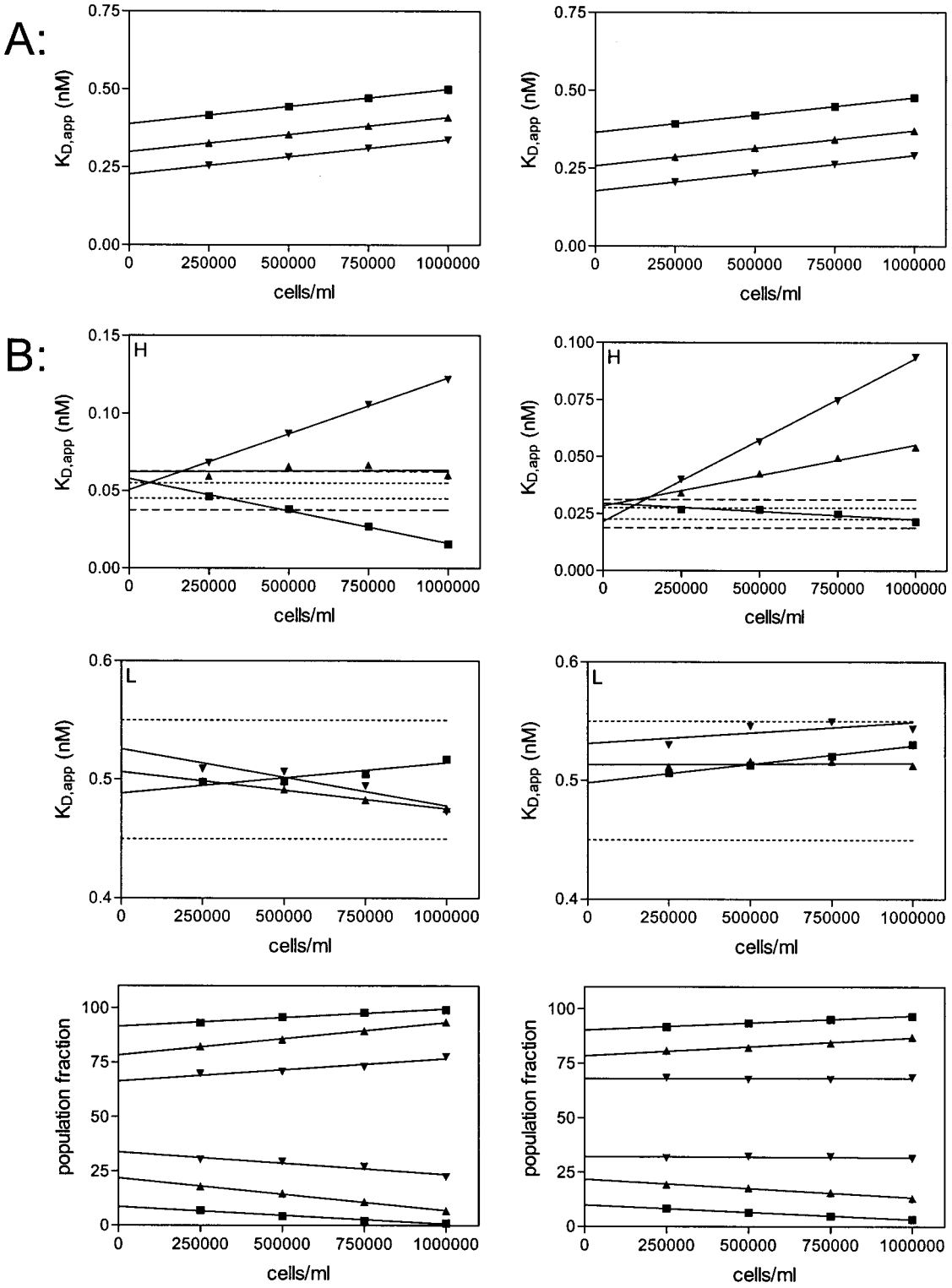


FIGURE 4: Fits of simulated data to two receptor classes. (A) Data simulated assuming a two-site model (eq 3) and fit using a one-site model (eq 2). (B) The same two-site data fit using a two-site model (eq 4). H corresponds to the high-affinity site, and L corresponds to the low-affinity site. The fractional receptor population is the fraction of the total binding sites that each population contributes. Examples in the left-hand column are for simulated data generated with $K_{D1} = 0.05$ nM and $K_{D2} = 0.5$ nM, and the right-hand column are for data generated with $K_{D1} = 0.025$ nM and $K_{D2} = 0.5$ nM. The total receptor concentration is 0.1 nM with the fraction of high-affinity receptor class equal to 10% (■), 20% (▲), and 30% (▼) with $1 \times 10^5$ receptors per cell. The ±10% error limits for the $K_D$'s are indicated by the dotted lines, while ±25% errors are indicated by the dashed lines. Unlike the one-receptor-site fits, slopes of the cell density dependence of the apparent $K_D$'s are not always positive.

this experiment. All data analysis was carried out on corrected data, an example of such is shown in Figure 5. The linear plot of the data and the associated fits to either the one- or the two-site model do not visually indicate which fit is most appropriate (Figure 5A). In contrast, the log plot of the data clearly shows that the data are better fit by the two-site model (Figure 5B). This is supported by statistical evaluation of the one- and two-site model fits and by a

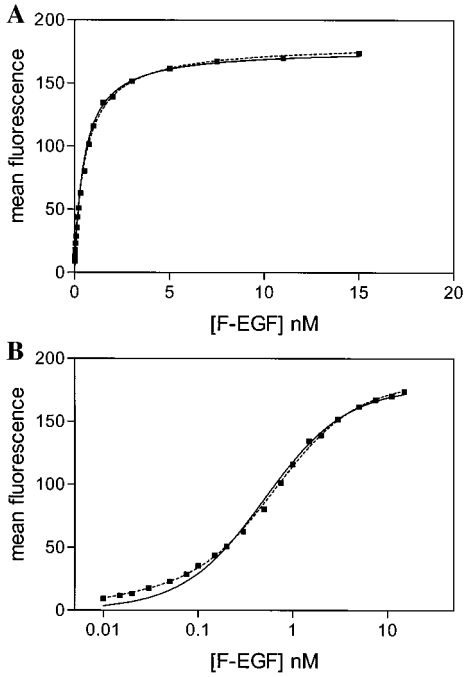


FIGURE 5: F-EGF binding isotherm. (A) Linear plot of mean fluorescence for one curve of F-EGF binding to EGF receptor in WT3 cells at $9.6 \times 10^5$ cells/mL and fits to one-site (solid line) and two-site (dashed line) models. The one-site fit yields a $K_{D,app}$ of 0.51 nM. The two-site fit to these data yields $K_{D,app}$'s of 0.008 and 0.66 nM with 6.8% of the total binding sites corresponding to the high-affinity site. (B) log plot of the same data as in (A). From the plot in (B), it is visually apparent that the two-site model is a better fit to the data than the one-site fit. An F-test of the two models yields a $p$-value of $<0.0001$, indicating that the two site-model is the better fit. The highest $p$-value for the remaining binding isotherms was 0.0003.

nonlinear Scatchard plot (data not shown), though as will be discussed below Scatchard plots are not an ideal method to analyze these data. F-EGF binding to WT3 cells was repeated at 10 additional cell densities. A plot of the $K_{D,app}$ versus cell density for a one-site fit is shown in Figure 6A. As discussed above, the data are relatively linear with regard to cell density; however, given the apparent multiple receptor populations present for EGF receptor expressed in 32D cells, the derived $K_D$ would not reflect the actual ligand binding that is occurring. Plots of the two $K_{D,app}$'s and the fraction of each site indicate that the $y$-intercept for the high-affinity site is ~20 pM and the $y$-intercept for the low-affinity site is near 0.4 nM, with the high-affinity site comprising ~20% of the receptor population (Figure 6A−C). These values are comparable to, though slightly higher in affinity than, previously determined values, measured by $^{125}$I-EGF binding, for the EGF receptor expressed in 32D cells (*48*).

## DISCUSSION

Many authors have examined various aspects of both direct ligand binding and competition binding assays. Many of these ligand binding studies have focused on the use of radiolabeled ligands and the issues associated with the use of these ligands; however, efforts to minimize the use of radioactivity have led to an increase in the use of fluorescently labeled ligands. Changes in the rotational properties (polarization/anisotropy) of fluorescent ligands upon binding to receptor have been exploited in ligand binding assays, and instruments designed to measure these changes are now commercially available. Alternatively, optical properties such as changes in fluorescence upon binding have also been used to measure both steady-state and kinetic parameters of ligand binding. In addition, pioneering work by Bohn (*30*) and Sklar (*31*) indicated the utility of flow cytometry in measuring ligand binding properties to intact cells, a method first exploited by Chatelier et al. (*32*) for the EGF receptor system. We have also exploited the advantages of flow cytometry to develop a straightforward method for measuring the $K_D$ of a ligand binding to a receptor. This approach utilizes multiple cell densities, and, while we apply this aproach to an assay using flow cytometry, the method is applicable to any ligand binding method.

Prior analyses of ligand binding data utilizing flow cytometry employed multiple cell densities to obtain binding affinity and number of receptors per cell (*31*, *32*). In the first analysis (*31*), multiple cell densities were used, and binding isotherms were obtained for each. The lowest cell density was fit to a one-site model to obtain the $K_{D,app}$, and then each isotherm was normalized to the maximal amount of binding from this fit, given in mean fluorescence units. For several selected ligand concentrations, the fractional amounts bound from these normalized isotherms were calculated and subsequently plotted versus cell concentration for each ligand concentration. An equation was derived for a one-site model that relates the cell concentration to the fractional amount bound, with a variable being the number of receptors per cell. This equation, in conjunction with the transformed, selected data plotted versus cell concentration, was used to estimate the number of receptors per cell. The limitations to this method are the need to normalize the data to the maximum amount bound, which might be in error depending on the extent of ligand depletion, and the restriction of this method to a one-site model.

In the second analysis, an isoparametric method was utilized to determine the binding affinities and number of receptors per cell (*32*). Similar to the first method, several binding isotherms using different cell densities were obtained. Then, several arbitrary mean fluorescence unit values were chosen. For each different binding isotherm, the ligand concentrations corresponding to these selected mean fluorescence values were determined. These values of ligand concentration were then plotted versus cell concentration. For each selected mean fluorescence value, the $y$-intercept corresponds to the free ligand concentration ($L_A$), and the slope corresponds to moles of ligand bound per mole of cells ($r$). The slope and intercepts from the multiple plots were then used to construct a Scatchard plot ($r/L_A$ versus $r$). The Scatchard plot was then used to determine if there were multiple binding populations and their affinities. This method requires multiple transformations of the data to determine from a Scatchard plot the binding affinity and the number of receptors per cell. Compared to the two methods described above, the method described in this paper, while yielding comparable results, is more straightforward, requiring no normalization of data and minimal manipulation of subsequent results.

That the $K_{D,app}$ becomes a better approximation for the intrinsic $K_D$ at lower cell densities arises from the simple fact that at lower cell densities there is less ligand depletion and parameters obtained from the use of eq 2 become better

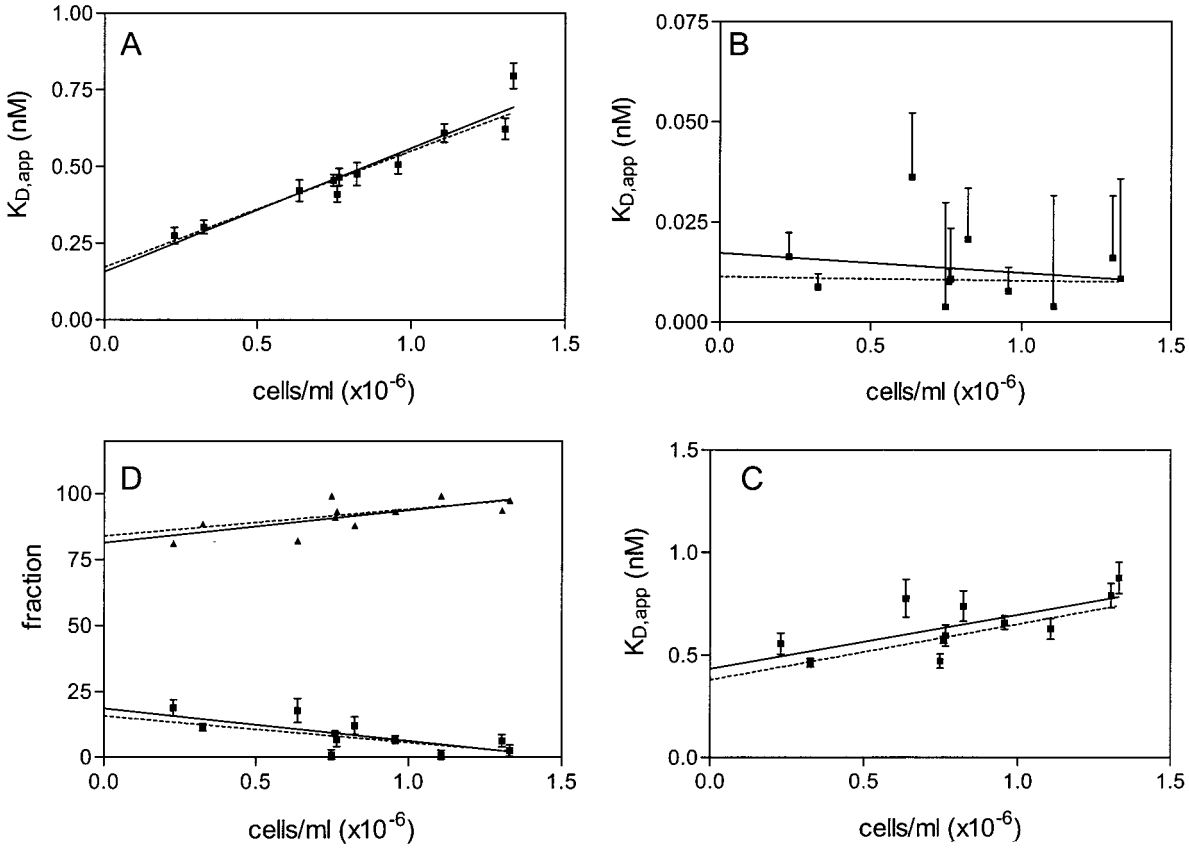


FIGURE 6: Plots of one-site and two-site models for F-EGF binding to EGF receptor. Shown are the parameters and estimated standard deviation from the one- and two-site model fits to the binding isotherms. Points that appear without error bars are due to the error being smaller than the symbol, and in panel B the error bars are only indicated in one direction. Regression was carried out on these data versus cell density with (dashed line) and without (solid line) weighting using the estimated standard deviations. (A) Plot of the $K_{D,app}$ for a one-site fit versus cell density. The *y*-intercepts are equal to 0.16 ± 0.04 nM (solid) and 0.17 ± 0.03 nM (dashed). (B) Plot of the $K_{D,app}$ for the high-affinity site yields *y*-intercepts equal to 0.017 ± 0.010 nM (solid) and 0.011 ± 0.003 nM (dashed). (C) Plot of the $K_{D,app}$ for the low-affinity site yields *y*-intercepts equal to 0.43 ± 0.10 nM (solid) and 0.38 ± 0.05 nM (dashed). (D) Plot of the fractions of the two affinities of F-EGF binding to the EGF receptor. The percentages of high-affinity sites are 18 ± 4% (solid) and 16 ± 3% (dashed). The errors for the *y*-intercepts are the standard errors from the regression analyses.

estimates of the true values. That different cell densities or protein concentrations can alter the reported $K_D$ values has been previously discussed. One study (*50*) derived a linear equation in which the *y*-intercept from a plot of $K_{D,app}$ versus receptor concentration yielded the true $K_D$ value. This derivation requires knowledge of the number of receptors per cell prior to obtaining the true $K_D$, whereas plotting the $K_{D,app}$ values versus cell density, as in our analysis, removes this requirement, and, in fact, can lead to the determination of the number of receptors per cell. In addition, the linear relationship between $K_{D,app}$ and receptor concentration is only valid if there is no ligand depletion. In a broad examination of ligand binding to dopamine receptors (*51*), the vast differences in affinities seen by different laboratories could be ascribed to the differences in the protein concentration of the membrane preparations used to measure binding. Though they did not attempt a mathematical fit, the data appeared to be linear at lower protein concentrations and had upward curvature as the protein concentration increased. These results are in agreement with our analysis indicating that the true relationship between cell density and $K_{D,app}$ is described by a second-order equation. That the derived $K_D$ values were dependent on the protein concentration of the membrane preparations is in agreement with the basic concept that at lower cell densities/receptor concentrations less ligand depletion occurs and the $K_{D,app}$ thus becomes a better approximation of the intrinsic $K_D$.

*General Ligand Binding.* While the simulations described under Results and the conclusions drawn from them were based on errorless data, introducing experimental error into the simulated data does not decrease the applicability of the method. Introducing 15% variability into the simulated data suggests that the experiment measuring $K_{D,app}$ at four different cell densities should be repeated at least 3 times to yield an accurate $K_D$ value from the *y*-intercept. While this may seem to be a large number of individual points to yield a single $K_D$ value, the relative simplicity of the assay makes the collection of the necessary data practical. Given the few steps involved in preforming the flow cytometry assay, error is primarily associated with the measurement of the cell densities and with pipetting. Due to the low error of each point, singlets can be utilized, compared to classical binding assays that employ duplicates or triplicates for each point to reduce error. A high enough number of ligand concentrations used to generate a single binding isotherm is required to minimize the effect of any one point on the fit; however, the choice of the number of ligand concentrations is no different in this case than in the case of an assay utilizing radioactivity. As a result, more ligand concentrations may be included in each individual assay without making the

experiment cumbersome. Based on these considerations, measuring binding over a range of cell densities, multiple times, to yield an accurate $K_D$ and an estimate of the number of receptors per cell is justified.

For cell lines expressing two receptor populations, extension of the method of using multiple cell densities allows for the determination of the $K_D$'s of the two binding affinities. Although the simulations indicate that the error associated with the high-affinity site may be higher than 10% (typically within 25%), the value obtained for the affinity of the high-affinity site is likely to be more accurate than would be obtained by using a single cell density (Figure 4). One important consideration in obtaining the multiple affinities and fractions is the ability of the fitting routine to assign the data to two unique populations. For example, the fitting routine in Prism is unable to obtain fits indicative of two sites at higher cell densities in which the fraction of the high-affinity site approaches zero (Figure 4). Two-site fits could be obtained by altering the starting parameters for the high- and low-affinity sites so that the starting values were lower than the simulated values. At even higher cell densities and/or higher number of receptors per cell than those used in Figure 4, the fitting routine was unable to obtain a unique two-site fit, with the fit appearing to be only one-site, regardless of the starting guesses. This is due to the larger extent of ligand depletion under these conditions.

One general method that has been used to indicate the presence of multiple receptor populations is the transformation and plot of Scatchard (*33*). A nonlinear Scatchard plot of binding data is indicative of ligand binding to more than one class of binding sites, including multiple binding sites on a single receptor, multiple receptor populations, or cooperative ligand binding. There are several considerations in using Scatchard plots to indicate the presence of multiple binding sites and to obtain their binding affinities and receptor populations. One consideration is the use of $L_F$ or $L_T$ in calculation of bound/free used in the Scatchard plot. Employing $L_F$, i.e., determining $L_F$ for each data point, will yield accurate binding affinities regardless of the extent of ligand depletion. However, use of $L_T$ as an estimate for $L_F$ in cases in which there is ligand depletion will lead to erroneous values for the binding affinities and receptor populations. A second consideration is the range and density of ligand concentrations used in the binding experiment. It is possible to obtain a curvilinear Scatchard plot but to have one of the populations defined by only two or three data points. While sufficient to describe a line, the parameters obtained from so few points are likely to yield inaccurate parameters. Moreover, despite yielding a curvilinear Scatchard plot, there may be no statistical justification to fitting the *nontransformed* data to a two-site model compared to a one-site model. Although two independent receptor populations may actually be present, if the nontransformed data alone do not support two populations, parameters obtained from the transformed data for two sites are likely to be inaccurate.

*F-EGF Binding to EGF Receptor.* Previous experiments have measured binding of EGF to the EGF receptor in a multitude of cell lines that express the EGF receptor both naturally or through transfection. EGF binding to EGF receptor often has yielded curvilinear Scatchard plots that are generally fit using a model consisting of two independent receptor populations, termed high- and low-affinity receptors. Of the previous reports of $^{125}$I-EGF binding to EGF receptors expressed in 32D cells (*48*, *52*−*54*), only one carried out a direct binding experiment (*48*), estimating 6000 (4%) high-affinity sites with a $K_D$ of 0.09 nM and 140 000 low-affinity sites with a $K_D$ of 2.1 nM.

Inherent in the two-site model is the assumption that the two receptor populations are independent of each other. When viewed in light of the physiology of the system, this would not appear to be the case for the EGF receptor, since addition of EGF to the receptors results in a measurable increase in receptor dimerization/aggregation, where dimers/aggregates of the receptor are often hypothesized to have a higher binding affinity than monomeric receptor. It has previously been noted that the two-independent-site model and receptor aggregation are inconsistent with typical concave-up Scatchard plots obtained for EGF binding to the EGF receptor (*55*). Even though there appears to be an inconsistency between the two-independent-site model and EGF receptor properties, the binding of F-EGF to the EGF receptor was fit using this model, because of its prevalence.

In this examination of EGF binding to the EGF receptor, the two-independent-site model yielded affinities (0.017 and 0.43 nM) and their respective populations (18% and 82%) from the intercepts of the cell density plots (Figure 6). The one remaining variable in the fits for this model is the number of receptors per cell. To obtain the number of receptors per cell, theoretical binding isotherms at various numbers of receptors per cell must be carried out. The two receptor populations ($R_T$ and $S_T$) are determined from the fraction of each population, the number of receptors per cell, and the cell density. These values, $R_T$ and $S_T$, are then used with the two $K_D$'s to obtain $R_F$ using eq 3a. The amount of free receptor, $R_F$, is then used in eq 3 to obtain the amount bound for each population of receptor, *RL* and *SL*, which are then combined to generate the total amount bound. This is done for four cell densities (250 000−1 000 000 cells/mL) for each chosen value of the number of receptors per cell. The four theoretical binding isotherms are then fit using eq 4, and the resultant fraction of each population is plotted versus cell density and compared to the experimental population fraction data. This was carried out for multiple values of the number of receptors per cell, and it was found that 125 000 receptors per cell yielded an adequate comparison of the simulated data to the experimental data (Figure 7A). This value is similar to the range ($5.0 \times 10^4$ to $1.0 \times 10^5$) obtained from multiple single-point $^{125}$I-EGF binding assays (data not shown). After obtaining an adequate correspondence between the simulated data and experimental data for the fraction plots, the plots of the $K_{D,app}$ for the simulated data for 125 000 receptors per cell were compared to the experimental data. Whereas the fraction plots were in agreement, the affinity plots for the simulated data are not in agreement with the experimental data (Figure 7B,C). One can obtain curves that agree with the affinity plots, but the data from these simulations no longer agree with the experimental data for the fraction plots. While each individual binding curve can be fit by the two-independent-site model, the changes in the parameters versus cell density are not consistent with this model. *This argues against the validity of the two-independent-site model for describing the EGF*−*EGF receptor system.*

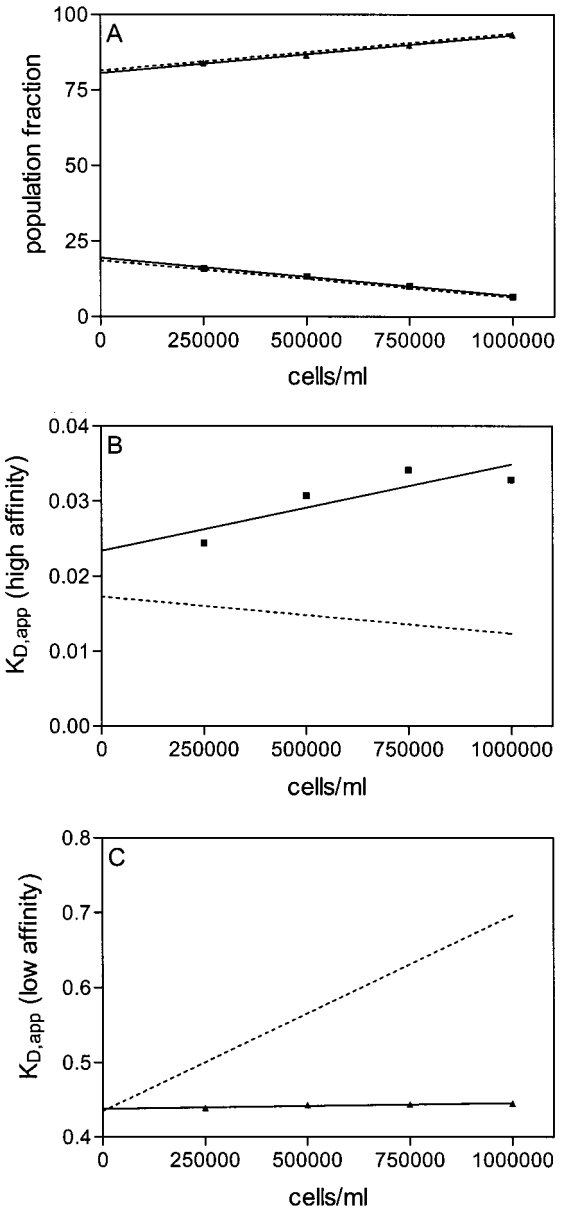


FIGURE 7: Comparison of simulated data to experimental data to obtain the number of receptors per cell. Data were simulated using eq 3 at four cell densities (250 000−1 000 000 cells/mL), using the two $K_D$'s and fractions from the fits with no weighting given in Figure 6, and 125 000 receptors per cell. These simulated data were fit using eq 4, and the parameters obtained from these fits are plotted versus cell density. The fraction of the two populations (A), the high-affinity site $K_{D,app}$ (B), and the low-affinity site $K_{D,app}$ (C) are shown. The dashed lines correspond to fits to the experimental data (Figure 6). The fraction plot (A) agrees with approximately 125 000 receptors per cell, whereas the two affinity plots (B, C) are inconsistent with this value. It is possible to obtain plots that are consistent with the affinity data, but then the fraction plots do not agree with the experimental data. The inability of the model to describe the overall experimental data argues against its validity in this system.

The experimental evidence presented here, that the two-independent-site model is not an accurate description of the binding of EGF to the EGF receptor, is consistent with experimental observations that the EGF receptor undergoes measurable changes in its states of oligomerization, phosphorylation, association with various downstream signaling molecules, etc., upon ligand binding, none of which are taken into account in this model. In a previous examination of ligand binding (*55*), a model was proposed that explicitly included receptor monomer−dimer interconversion:

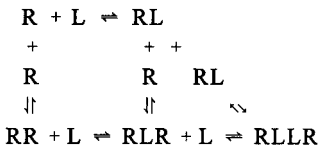


This model allows for binding of ligand to both monomers (R) and dimers (RR). In deriving the equations, it was assumed that there was no ligand depletion, and to obtain adequate fits of this model to the data, some equilibrium constants were fixed (*55*), suggesting that this model has too many individual binding steps to allow for determination of the binding constants from a simple equilibrium binding experiment. Another possible model, which is a subset of the above model:

$$R + R \rightleftharpoons RR + L \rightleftharpoons RRL + L \rightleftharpoons RRLL$$

only allows binding of ligand to a dimer (RR). These two models have been used to fit the experimental data presented here, assuming no ligand depletion, and the models yield equivalent fits to the data (data not shown), suggesting that neither model is better than the other. This is interesting, considering the one model assumes ligand binding to monomers and dimers, while the other assumes ligand binding to dimers only. Perhaps neither model accurately describes binding of EGF to the EGF receptor, because neither model accounts for phosphorylation, potential receptor conformational changes, or additional protein−protein interactions that might affect ligand binding.

Any multistep binding model will contain a number of equilibrium constants that will not easily be determined from a single equilibrium binding experiment. It is more likely that multiple experiments will be needed to isolate the various steps. The combination of these experiments should lead to a more complete picture of EGF binding to the EGF receptor. While the focus of this discussion is on EGF binding to the EGF receptor, these issues also apply to the whole ErbB family, and to any receptor system that exhibits multiple binding states.

## ACKNOWLEDGMENT

We thank Dr. G. N. Gill for the pXER plasmid, Dr. G. Carpenter for the 32D and WEH1-3B cells, and Drs. L. E. Limbird, R. C. Williams, and A. H. Beth for their critical reading of drafts of the manuscript. We are indebted to Professor G. Webb for his assistance in constructing the Mathematica routines for competition binding experiments (in Suporting Information).

## SUPPORTING INFORMATION AVAILABLE

This material discusses competition experiments utilizing similar methods as those described for the direct binding measurement (15 pages). This material is available free of charge via the Internet at http://pubs.acs.org.

## REFERENCES

1. Ullrich, A., Coussens, L., Hayflick, J. S., Dull, T. J., Gray, A., Tam, A. W., Lee, J., Yarden, Y., Libermann, T. A., Schlessinger, J., et al. (1984) *Nature 309*, 418−425.

2. Stein, R. A., and Staros, J. V. (2000) *J. Mol. Evol. 50*, 397−412.
3. Coussens, L., Yang-Feng, T. L., Liao, Y. C., Chen, E., Gray, A., McGrath, J., Seeburg, P. H., Libermann, T. A., Schlessinger, J., Francke, U., et al. (1985) *Science 230*, 1132−1139.
4. Kraus, M. H., Issing, W., Miki, T., Popescu, N. C., and Aaronson, S. A. (1989) *Proc. Natl. Acad. Sci. U.S.A. 86*, 9193−9197.
5. Plowman, G. D., Whitney, G. S., Neubauer, M. G., Green, J. M., McDonald, V. L., Todaro, G. J., and Shoyab, M. (1990) *Proc. Natl. Acad. Sci. U.S.A. 87*, 4905−4909.
6. Plowman, G. D., Culouscou, J. M., Whitney, G. S., Green, J. M., Carlton, G. W., Foy, L., Neubauer, M. G., and Shoyab, M. (1993) *Proc. Natl. Acad. Sci. U.S.A. 90*, 1746−1750.
7. Heimberg, M., Weinstein, I., LeQuire, V. S., and Cohen, S. (1965) *Life Sci. 4*, 1625−1633.
8. Cohen, S. (1965) *Dev. Biol. 12*, 394−407.
9. Gray, A., Dull, T. J., and Ullrich, A. (1983) *Nature 303*, 722−725.
10. Derynck, R., Roberts, A. B., Winkler, M. E., Chen, E. Y., and Goeddel, D. V. (1984) *Cell 38*, 287−297.
11. Shing, Y., Christofori, G., Hanahan, D., Ono, Y., Sasada, R., Igarashi, K., and Folkman, J. (1993) *Science 259*, 1604−1607.
12. Shoyab, M., McDonald, V. L., Bradley, J. G., and Todaro, G. J. (1988) *Proc. Natl. Acad. Sci. U.S.A. 85*, 6528−6532.
13. Toyoda, H., Komurasaki, T., Uchida, D., Takayama, Y., Isobe, T., Okuyama, T., and Hanada, K. (1995) *J. Biol. Chem. 270*, 7495−7500.
14. Higashiyama, S., Abraham, J. A., Miller, J., Fiddes, J. C., and Klagsbrun, M. (1991) *Science 251*, 936−939.
15. Holmes, W. E., Sliwkowski, M. X., Akita, R. W., Henzel, W. J., Lee, J., Park, J. W., Yansura, D., Abadi, N., Raab, H., Lewis, G. D., et al. (1992) *Science 256*, 1205−1210.
16. Wen, D., Peles, E., Cupples, R., Suggs, S. V., Bacus, S. S., Luo, Y., Trail, G., Hu, S., Silbiger, S. M., Levy, R. B., et al. (1992) *Cell 69*, 559−572.
17. Chang, H., Riese, D. J., II, Gilbert, W., Stern, D. F., and McMahan, U. J. (1997) *Nature 387*, 509−512.
18. Carraway, K. L., III, Weber, J. L., Unger, M. J., Ledesma, J., Yu, N., Gassmann, M., and Lai, C. (1997) *Nature 387*, 512−516.
19. Zhang, D., Sliwkowski, M. X., Mark, M., Frantz, G., Akita, R., Sun, Y., Hillan, K., Crowley, C., Brush, J., and Godowski, P. J. (1997) *Proc. Natl. Acad. Sci. U.S.A. 94*, 9562−9567.
20. Harari, D., Tzahar, E., Romano, J., Shelly, M., Pierce, J. H., Andrews, G. C., and Yarden, Y. (1999) *Oncogene 18*, 2681−2689.
21. Alroy, I., and Yarden, Y. (1997) *FEBS Lett. 410*, 83−86.
22. Shoyab, M., De Larco, J. E., and Todaro, G. J. (1979) *Nature 279*, 387−391.
23. Magun, B. E., Matrisian, L. M., and Bowden, G. T. (1980) *J. Biol. Chem. 255*, 6373−6381.
24. King, A. C., and Cuatrecasas, P. (1982) *J. Biol. Chem. 257*, 3053−3060.
25. Baker, J. B., and Cunningham, D. D. (1978) *J. Supramol. Struct. 9*, 69−77.
26. Ullrich, A., and Schlessinger, J. (1990) *Cell 61*, 203−212.
27. Tzahar, E., Waterman, H., Chen, X., Levkowitz, G., Karunagaran, D., Lavi, S., Ratzkin, B. J., and Yarden, Y. (1996) *Mol. Cell. Biol. 16*, 5276−5287.
28. Fitzpatrick, V. D., Pisacane, P. I., Vandlen, R. L., and Sliwkowski, M. X. (1998) *FEBS Lett. 431*, 102−106.
29. Sliwkowski, M. X., Schaefer, G., Akita, R. W., Lofgren, J. A., Fitzpatrick, V. D., Nuijens, A., Fendly, B. M., Cerione, R. A., Vandlen, R. L., and Carraway, K. L., III (1994) *J. Biol. Chem. 269*, 14661−14665.
30. Bohn, B. (1980) *Mol. Cell. Endocrinol. 20*, 1−15.
31. Sklar, L. A., and Finney, D. A. (1982) *Cytometry 3*, 161−165.
32. Chatelier, R. C., Ashcroft, R. G., Lloyd, C. J., Nice, E. C., Whitehead, R. H., Sawyer, W. H., and Burgess, A. W. (1986) *EMBO J. 5*, 1181−1186.
33. Scatchard, G. (1949) *Ann. N.Y. Acad. Sci. 51*, 660−672.
34. Rosenthal, H. E. (1967) *Anal. Biochem. 20*, 525−532.
35. Norby, J. G., Ottolenghi, P., and Jensen, J. (1980) *Anal. Biochem. 102*, 318−320.
36. Klotz, I. M. (1982) *Science 217*, 1247−1249.
37. Zierler, K. (1989) *Trends Biochem. Sci. 14*, 314−317.
38. Wang, Z. X., and Jiang, R. F. (1996) *FEBS Lett. 392*, 245−249.
39. Rousseau, D. L., Jr., Guyer, C. A., Beth, A. H., Papayannopoulos, I. A., Wang, B., Wu, R., Mroczkowski, B., and Staros, J. V. (1993) *Biochemistry 32*, 7893−7903.
40. Taylor, J. M., Mitchell, W. M., and Cohen, S. (1972) *J. Biol. Chem. 247*, 5928−5934.
41. Rousseau, D. L., Jr., Staros, J. V., and Beechem, J. M. (1995) *Biochemistry 34*, 14508−14518.
42. Laemmli, U. K. (1970) *Nature 227*, 680−685.
43. Sklar, L. A., Finney, D. A., Oades, Z. G., Jesaitis, A. J., Painter, R. G., and Cochrane, C. G. (1984) *J. Biol. Chem. 259*, 5661−5669.
44. Schwartz, A., and Fernandez-Repollet, E. (1994) *Methods Cell Biol. 42*, 605−626.
45. Wang, L. M., Kuo, A., Alimandi, M., Veri, M. C., Lee, C. C., Kapoor, V., Ellmore, N., Chen, X. H., and Pierce, J. H. (1998) *Proc. Natl. Acad. Sci. U.S.A. 95*, 6809−6814.
46. Pierce, J. H., Ruggiero, M., Fleming, T. P., Di Fiore, P. P., Greenberger, J. S., Varticovski, L., Schlessinger, J., Rovera, G., and Aaronson, S. A. (1988) *Science 239*, 628−631.
47. Pinkas-Kramarski, R., Soussan, L., Waterman, H., Levkowitz, G., Alroy, I., Klapper, L., Lavi, S., Seger, R., Ratzkin, B. J., Sela, M., and Yarden, Y. (1996) *EMBO J. 15*, 2452−2467.
48. Fazioli, F., Minichiello, L., Matoska, V., Castagnino, P., Miki, T., Wong, W. T., and Di Fiore, P. P. (1993) *EMBO J. 12*, 3799−3808.
49. Nakamura, N., Chin, H., Miyasaka, N., and Miura, O. (1996) *J. Biol. Chem. 271*, 19483−19488.
50. Chang, K. J., Jacobs, S., and Cuatrecasas, P. (1975) *Biochim. Biophys. Acta 406*, 294−303.
51. Seeman, P., Ulpian, C., Wreggett, K. A., and Wells, J. W. (1984) *J. Neurochem. 43*, 221−235.
52. Tzahar, E., Pinkas-Kramarski, R., Moyer, J. D., Klapper, L. N., Alroy, I., Levkowitz, G., Shelly, M., Henis, S., Eisenstein, M., Ratzkin, B. J., Sela, M., Andrews, G. C., and Yarden, Y. (1997) *EMBO J. 16*, 4938−4950.
53. Tzahar, E., Moyer, J. D., Waterman, H., Barbacci, E. G., Bao, J., Levkowitz, G., Shelly, M., Strano, S., Pinkas-Kramarski, R., Pierce, J. H., Andrews, G. C., and Yarden, Y. (1998) *EMBO J. 17*, 5948−5963.
54. van de Poll, M. L., van Vugt, M. J., Lenferink, A. E., and van Zoelen, E. J. (1998) *J. Biol. Chem. 273*, 16075−16081.
55. Wofsy, C., Goldstein, B., Lund, K., and Wiley, H. S. (1992) *Biophys. J. 63*, 98−110.


BI002817A